Title: The effects of inclination angle on Archimedes screw generator power production with constant head

Published as:

Simmons S, Dellinger G, Lyons M, Terfous A, Ghenaim A, Lubitz WD. Effects of inclination angle on Archimedes screw generator power production with constant head. Journal of Hydraulic Engineering. 2021 Mar 1;147(3):04021001. on Archimedes screw generator power production with constant head. Journal of Hydraulic Engineering. 2021 Mar 1;147(3):04021001.

Manuscript Number:

MS HYENG-12253

Authors:

Simmons, Scott

Doctoral Candidate, University of Guelph, Guelph, Ontario, Canada, N1G 2W1

ssimmons@uoguelph.ca

Dellinger, Guilhem

Associate Professor, ICUBE (UMR 7357) – ENGEES, Strasbourg, France, 67070 Strasbourg

guilhem.dellinger@engees.unistra.fr

Lyons, Murray

Research Associate, University of Guelph, Guelph, Ontario, Canada, N1G 2W1

murrayly@uoguelph.ca

Terfous, Abdelali

Associate Professor, ICUBE (UMR 7357) – INSA, Strasbourg, France, 67000 Strasbourg

abdelali.terfous@insa-strasbourg.fr

Ghenaim, Abdellah

Associate Professor, ICUBE (UMR 7357) – INSA, Strasbourg, France, 67000 Strasbourg

abdellah.ghenaim@insa- strasbourg.fr

Lubitz, William David **(Corresponding Author)**

Associate Professor, University of Guelph, Guelph, Ontario, Canada, N1G 2W1

wlubitz@uoguelph.ca

Keywords:

Archimedes screw, screw generator, computational fluid dynamics, inclination angle, micro-hydropower

Abstract:

Three laboratory-scale Archimedes screw generators were tested for their power production. They were tested at different inclination angles corresponding to their lengths in order to maintain a constant head for each screw. Experimentation was used to develop initial insight into the effect of inclination angle on Archimedes screw power production. Computational fluid dynamic simulations were then compared to the experimental data and evaluated for their accuracy. The model was found to be acceptable and was then used to extend the dataset to a total of 7 inclination angles across the range of $\beta = 10°$ to $40°$. It was found that Archimedes screw generators with shallower inclination angles produce more power. It is noted that shallower inclination angles correspond to longer screws and thusly more civil infrastructure costs. So, the authors suggest that the ideal inclination angle for an Archimedes screw generator installation is between $\beta = 20°$ and $25°$ based on this laboratory-scale testing.

1. Introduction

The Archimedes screw is an ancient technology that was developed to pump water from lower to higher elevations. It has been used as a hydropower generator (as an "Archimedes screw generator" or "ASG") since the early 1990's (Radlik 1997). As such, much of its design and implementation is experience-driven and could potentially be optimized through experimental study and analysis. This paper will discuss the optimization of the inclination angle design parameter for ASGs to improve mechanical performance.

Archimedes screws have very simple and robust geometries. They are a helical array of blades wrapped around a central cylindrical tube and are often described by their outer diameter (D_o), inner diameter (D_i), pitch (S), flighted length (L), number of blades (N), and inclination angle (β) (Figure 1). When operating as a generator, water enters the top of the inclined screw at an inlet water level (h_U) and begins filling the spaces in between each successive blade - forming a "bucket" of water (Rorres 2000). Each bucket of water imparts a distribution of hydrostatic pressure on the screw blades which generates a torque and rotates the screw, the screw's shaft, and an electric generator. As the screw turns, the buckets of water translate along the screw's trough and get deposited back into the main streamflow at the bottom of the screw. It should be noted that, due to this robust design, sediment, debris, and even aquatic flora and fauna can pass through the screw unharmed (Havn et al. 2017; Kibel 2008; McNabb et al. 2003) – which is one of the reasons that the technology has become more attractive in the micro-hydropower sector (Simmons and Lubitz 2017).

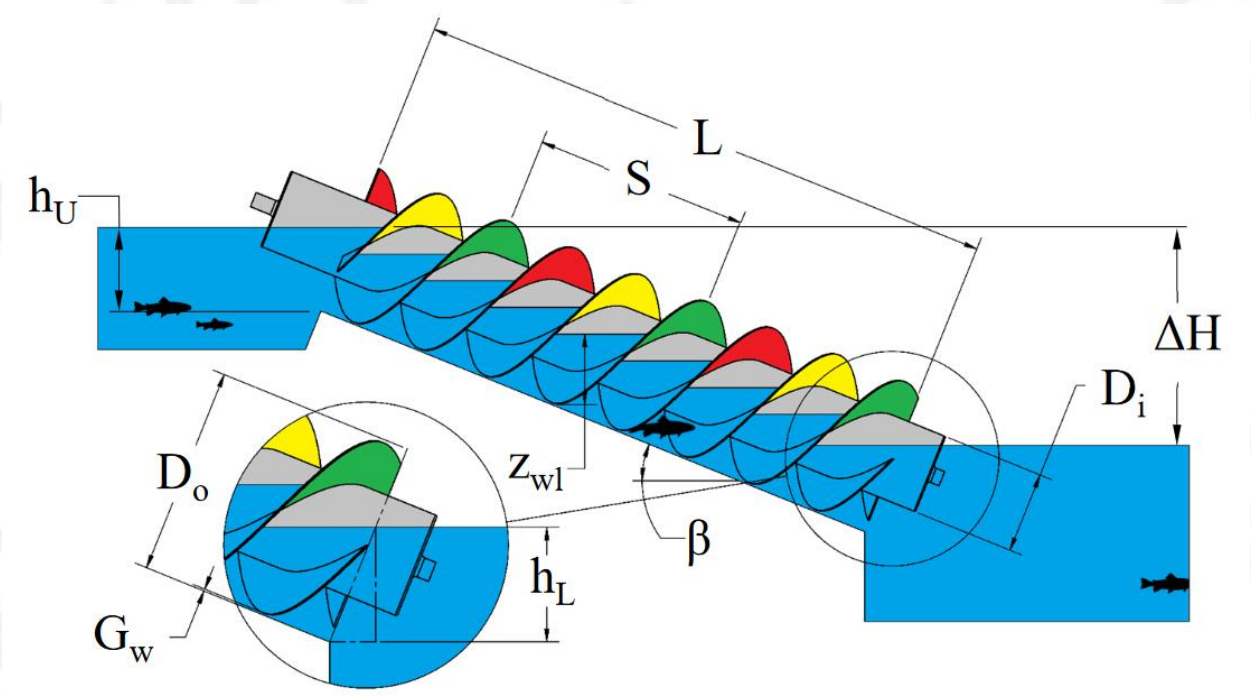

Figure 1: Archimedes screw generator geometry.

A real-world ASG plant usually operates at river-to-wire efficiencies between 60% and 80% (Kozyn et al. 2015; Lashofer et al. 2012), while some well-designed installations can operate at even greater efficiencies (Lyons and Lubitz 2013). Some work has been done in the literature to predict Archimedes screw generator performance (Kozyn 2016; Lubitz et al. 2014; Müller and Senior 2009; Nuernbergk 2012), though much of the work lacks robust experimental validation. There are some experimental studies in the literature that seem to agree well with much of the theory presented in the aforementioned models, but much of the data is on small, laboratory-scale screws (Dellinger et al. 2016b; Hawle et al. 2012; Khan et al. 2018; Kozyn 2016; Rohmer et al. 2016; Simmons et al. 2017; Songin 2017; Songin and Lubitz 2018). Computational fluid dynamics has been implemented to extend some of the data in the literature, allowing researchers to visualize flow patterns within the screw and quantify the performance of different geometry screws without having to manufacture them (Dellinger et al. 2016a, 2018a; b; Simmons 2018).

There are a few studies in the literature that explore the effect of screw geometry on hydropower production. Songin (Songin 2017) carried out laboratory-scale experiments to see the effects of varying screw length, number of blades, inner and outer diameter, pitch, and outlet fill height (h_L). A few conclusions were drawn that seemed to match the industry standard for ASG design. For example, it was found that a diameter ratio of $D_i/D_o \approx 0.5$ performed most efficiently. This value was also found when a Bayesian Optimization study was carried out on the screw's design (Lisicki et al. 2016). This diameter ratio is very commonly used in industry (Lashofer et al. 2012), and that is most likely because it was the most optimal design for an Archimedes screw when operating as a pump (Nagel 1968; Rorres 2000).

Songin also found that the screw performed most efficiently when about 60% of the outlet was submerged (i.e. $h_L/D_o \cos\beta = 0.60$) (Songin 2017). Experience suggests that many ASG installations have an outlet fill height of about 50-60% when the screw is operating at its design flow and head. It seems that some manufacturers recognize the potential efficiency improvements of maintaining this outlet fill level even as receiving basin water levels vary, and have installed varying inclination ASGs, for example, at the Romney Weir plant on the Thames River in Windsor, UK. The lower end of a screw can be raised or lowered by a hydraulic cylinder to maintain a consistent outlet immersion level. There is a lack of robust evidence in the literature to show if this is economically advantageous or not.

Another design parameter that has been investigated briefly in the literature is the inclination angle β (or slope) of the screw. The authors previously published a paper exploring the effects of inclination angle on ASG performance (Dellinger et al. 2018b). The inclination angle of a single laboratory-scale screw was set to three inclination angles (β = 20, 24.5, and 29°) to observe how the mechanical efficiency of the ASG was affected. The data set was extended using computational fluid dynamic (CFD) simulations to observe a wider range of inclinations (β = 10, 15.5, 20, 24.5, 29, 33.5, and 38°) and the effect of adding more blades on screw performance. The β = 15.5° simulation had the highest efficiency. However, in a real-world installation the available head and flow rate would be defined by the site. So,

as the inclination angle of a proposed screw design changes, the length of the screw L would change to match the site head ΔH. As such, the authors decided that it would be valuable to follow-up with a study that maintained constant head and constant flow rate but varied the inclination angle of the ASGs (cf. Figure 3).

This paper presents data collected experimentally (on small, laboratory-scale ASGs) for varying inclination angle with constant head. This was done by testing a set of three screws that were identical except for length, so that if the screws were installed at the same head, each screw would have a different inclination angle. As well, computational fluid dynamic (CFD) simulations were used to extend the dataset to other inclination angles and different sized screws. The lab-scale data was used to evaluate the CFD model's accuracy and draw some conclusions. The CFD simulations were then used to simulate a wider range of conditions that were not possible to test experimentally.

2. Experimental Methods

Experiments were carried out in the University of Guelph's Archimedes screw laboratory. The lab houses a test rig that runs a recirculating pump through a series of water basins. Figure 2 shows the screws position within the system, it is placed between an upper and lower basin. A weir basin is used provide secondary flow measurements at the inflow to the upper basin. A recirculating water loop started in the lower basin, where a variable speed pump was used to pump water from the end of the lower receiving basin up to the weir basin through a long, straight return pipe. An Omega FTB-740 inline turbine flow meter was located midway along the return pipe and measured the flow rate with an accuracy of $\pm$1% FS. Water entered the weir basin through a perforated tube and upfilled to the weir crest. It spilled through two Cipoletti weirs and into the upper basin; the water depth in the weir basin was measured and used with a calibration curve to redundantly measure flow through the system. The water then passed through an Archimedes screw from the upper basin into the lower basin where it

began the recirculation again. Two Keller Series 26 Y depth sensors (0.25% FS accuracy) were installed in stilling wells in the upper and lower basins to measure the head.

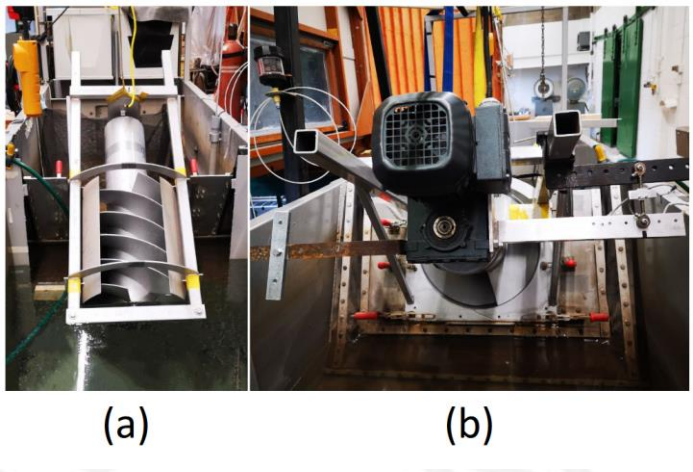

Figure 2: the University of Guelph's Archimedes screw laboratory setup. The screw is placed between an upper and lower basin (a) and a VFD motor is mounted on the top end (b) to control speed and measure torque using a strain gauge and torque arm.

A torque arm with a mounted strain gauge was attached to the ASG's trough framework and a Variable Frequency Drive (VFD) motor to measure the torque about the screw's rotational axis (Figure 2 (b)). The torque measurement apparatus had an overall uncertainty of $\delta T = 0.22\ Nm$ (Simmons 2018). The VFD was used to control the rotational speed of the screw, and a magnetic tachometer was used at a very high sample rate to measure and record the speed. The sample rate of the tachometer was above 1000 Hz and the rotational speed of the screw was no greater than 100 RPM, therefore the uncertainty in the rotational speed measurements were neglected. A handheld tachometer was often used to verify the measurements. Once both the torque and rotational speed were measured, the mechanical power at the shaft was calculated (i.e. the power that would be available to turn an electric generator in a real-world installation). Since the flow rate and the upper and lower water levels were also measured, the hydraulic power in the water was calculated, and the efficiency of the screw was determined. The total uncertainty in efficiency measurements was found to be about $\delta\eta_{avg} \approx \pm 0.054$ or $\pm\ 5.4\%$.

The system was instrumented with a pressure tap in the screw trough at the bottom centre location midway down the screw to measure the water level (z_{wl}) in the buckets of the screw (Songin and Lubitz, 2019). To verify the measurement was successful, the experimenter visually inspected the fill height during operation and documented it with a photograph. A DSLR camera was mounted to the test rig to consistently photograph and document the screw's filling patterns. The dimensionless fill height ratio (f) was calculated from the bucket water level using Eqn. 1, where the maximum and minimum water level in the bucket are z_{max} and z_{min}, respectively (cf. Figure 3).

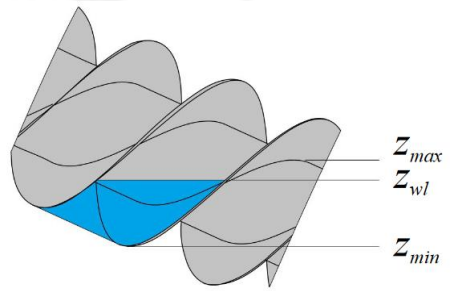

Figure 3: maximum (zmax), minimum (zmin), and actual (zwl) water levels in an Archimedes screw bucket.

The fill height ratio is then (Songin and Lubitz 2018):

$$f = \frac{z_{wl} - z_{min}}{z_{max} - z_{min}} \quad (1)$$

Essentially, when the fill height ratio is $f = 1$ the screw is full, and when $f = 0$, the screw is empty. Theoretically, the optimal fill height for a screw is $f = 1$, although it has been shown experimentally that this is not always the case (Songin and Lubitz 2018).The fill height ratio will exceed unity for instances of overflow leakage, when water overtops the inner cylinder of the screw.

The authors have selected the baseline inclination angle to be 24.4° to match previous experiments in the literature (Lyons 2014) and fit within the wide range of ASG inclination angles seen in practice. Based on Lashofer's Archimedes screw site map (Lashofer 2019) and previous study (Lashofer et al.

2012) the inclination angle of most ASGs is $\beta = 22°$ to $26°$, with some extreme values (e.g. $\beta = 30°$). Details from a few full-scale installations are shown in Table 1.

The University of Guelph Archimedes screw laboratory has 16 laboratory-scale Archimedes screws. This study used the three screws in Table 2 (termed the short, medium, and long screws) that match in every parameter except overall length.

The medium length screw was selected as the baseline screw so that a steeper and shallower screw could be tested. The inclination angles of the screws needed for a consistent head were found using basic trigonometry: the opposite side of the triangle from the inclination angle was kept constant (i.e. the head was constant) and the inclination angle was solved corresponding to its respective hypotenuse length (i.e. the length of the inclined screw) (cf. Figure 4). If the medium-length screw is installed at 24.4°, then the corresponding inclination angles of the short and long screws were 33.8° and 15.6°, respectively.

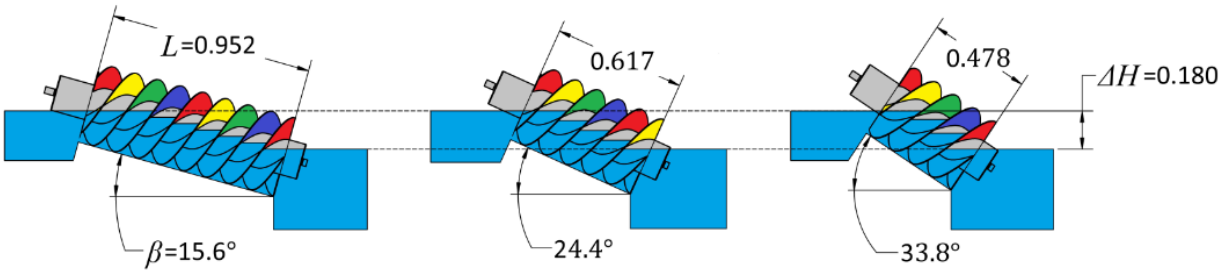

Figure 4: from left to right: the long, medium, and short screws shown with their respective lengths and inclination angles.

As mentioned above, ASGs operate with higher efficiencies when the outlet is nearly 60% submerged, and so this value was maintained throughout all tests and simulations. During experimentation it was difficult to maintain a constant head difference across the screw since the upper water level (h_U) was dependent on the rotational speed of the screw and the flow rate. So, tests were carried out for each of the three screws at the same flow rate and across the same range of rotational

speeds (15 to 60 RPM). The results were then processed to find the corresponding rotational speeds for each screw to operate with the desired head. Those points were then compared against each other and used to develop the CFD experiments.

The first tests were carried out to experimentally determine the flow rate that was to stay constant across all tests and simulations. The medium screw was installed in the test rig and experiments were carried out with the recirculated flow rate set to 9, 9.5, 10, 10.5, and 11 L/s through a range of 30 RPM to 39 RPM. For each test, the test rig was set to a flow rate, rotational speed, and an outlet fill height of 60% and sampled for one minute. The collected data from a test was time-averaged over the sample period and used to generate one data point. This helped to eliminate the variability caused by sloshing of water and other dynamic effects. Figure 5 shows the resulting measured mechanical efficiency with respect to screw rotational speed for each of the five flow rates. It was noted that the highest efficiency point seemed to shift to a higher rotational speed as the flow rate increased.

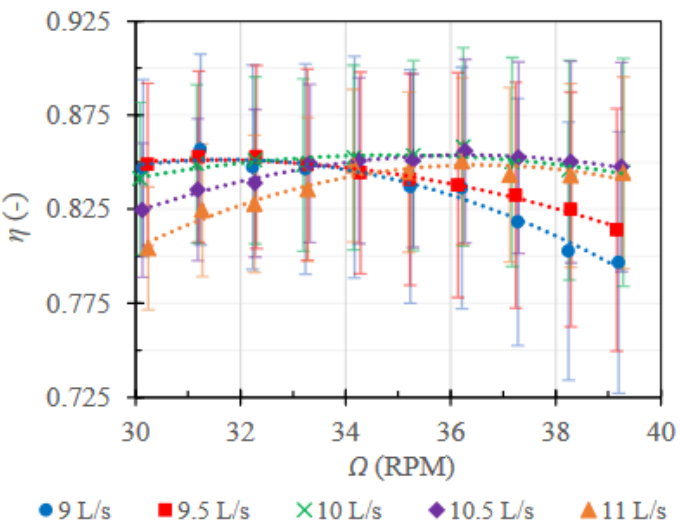

Figure 5: determining the optimal flow rate and rotational speed (Ω) for the medium length screw and the subsequent studies on both the long and short screws. The mechanical efficiency (η) is plotted against the rotational speed of the installation.

As can be seen, the uncertainty was high enough ($\eta_{avg} \approx \pm 0.054$) that any of the five flow rates could be reasonably assumed to contain the most efficient point. Measurement uncertainty was high due to propagation of uncertainties from multiple independent measurements through the calculations; efficiency is a function of the head (based on two water depth measurements), flow rate, torque, and rotational speed measurements. However, the most efficient points were sampled multiple times and the results were highly repeatable – suggesting actual measurement error may be smaller.

Due to the high uncertainty, some previous experimental worked was used to help suggest a flow rate for these tests. In some earlier experimentation the medium screw was tested along flow rates of 6, 8, 10, 12, and 14 L/s; it had its highest efficiencies at approximately 10 L/s (Simmons et al. 2017). So, the flow rate of 10 L/s was selected for the remaining experiments and simulations. The two remaining screws were tested through the same range of rotational speeds. Immediately prior to testing, each screw was maintained, balanced and had new bearings installed. The same one-minute time-averaged sampling technique was used for each data point.

3. Experimental Results

The results of this study will be presented in a few different sections. First, the results of the laboratory experiment are presented. Then, the CFD model will be used to simulate a subset of datapoints for validation. The results of the extended CFD dataset will be presented in Section 5 following the discussion of the CFD model setup and implementation. Discussions of the experimental and simulation results will be carried out together at the end of the paper.

The experiments were carried out on three different length screws with corresponding inclination angles that maintained the geometric head ($h_G = L \sin \beta$) across the screws. The results of these experiments are shown in Figure 6, where the measured mechanical efficiency (accounting for all losses

in the system; i.e. gap leakage, overflow leakage, etc.) is compared against the rotational speed for each screw.

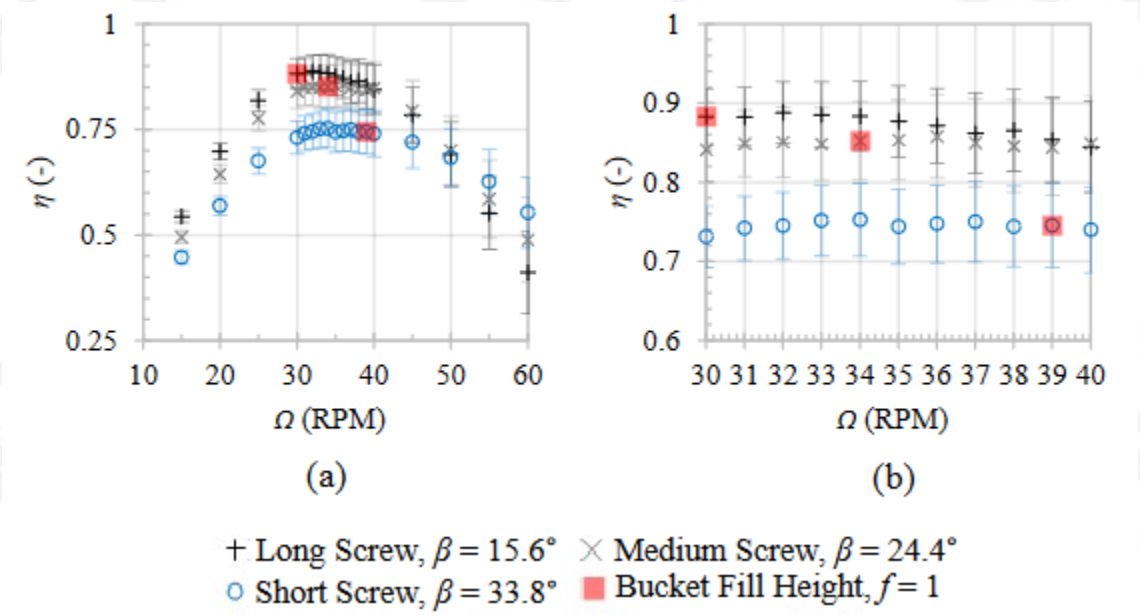

Figure 6: mechanical efficiency (η) with respect to rotational speed (Ω) of the long, medium, and short screws for a 10 L/s flow rate with fill height ratios of f = 1 highlighted for reference. The left plot (a) shows the full range of rotation speeds while the right plot (b) magnifies the plot to show the higher resolution data points clearly.

Figure 6 demonstrates that the longest screw (with $\beta = 15.6°$) performed with the highest overall efficiency. As the inclination angle increased (and the screw shortened) the overall efficiency decreased. However, it was interesting to see that the steeper inclination lead to the highest efficiency occurring at somewhat higher rotational speed; this was in part due to the changing bucket geometry. As the screw inclination angle increased the total water volume in a full bucket decreased (cf. Figure 7).

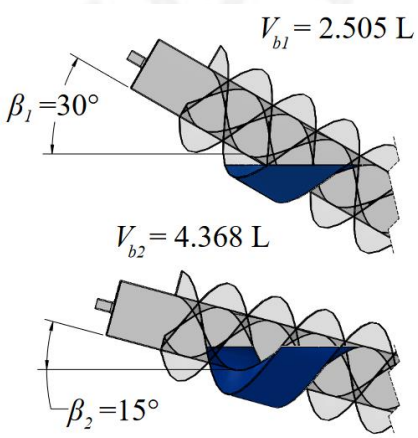

Figure 7: effect of inclination angle on total bucket volume of a full bucket (i.e., f = 1).

In Figure 6, points are highlighted that have a fill height ratio of unity. At lower rotational speeds, the fill height ratio exceeded unity (i.e. $f > 1$), meaning the screws began to exhibit overflow leakage. When the rotation speed of the screw was low, the water level of the buckets filled higher, the upper water level backed up, and there were significant overflow leakage losses.

As the rotation speed increased, less overflow leakage occurred. High rotation speed corresponded to lower bucket water levels as the screw began to "outrun" the speed of water filling into the first bucket. Overflow leakage occurred at different rotation speeds depending on the inclination of the screw, with the least overflow occurred in the screw with the lowest inclination angle. For example, overflow leakage was no longer present in the longest screw at speeds above 30 RPM, while in the shortest screw (with $\beta = 33.8°$) overflow ceased at speeds above 39 RPM.

To explore the effect of the changing bucket volumes, a pressure tap was used to measure the water depth of each screw halfway along the trough bottom (i.e. at a point where the bucket should be fully formed). More details on the pressure tap and fill height measurements at the University of Guelph Archimedes screw laboratory may be found in (Songin and Lubitz 2018). Figure 8 plots the dimensionless water depth measured immediately above the pressure tap sensor installed on the screw troughs for the short, medium, and long screw's most efficient operating points (cf. Figure 6). Since the sensor was

fixed on the trough, it caught the high and low water depths in the bucket due to the inclined geometry. It should be noted that Figure 8 shows the measurement of time-varying water depth above a specific point along the screw's length; these values may be time-averaged to find the fill height ratio (f) for each screw under the specified operating conditions.

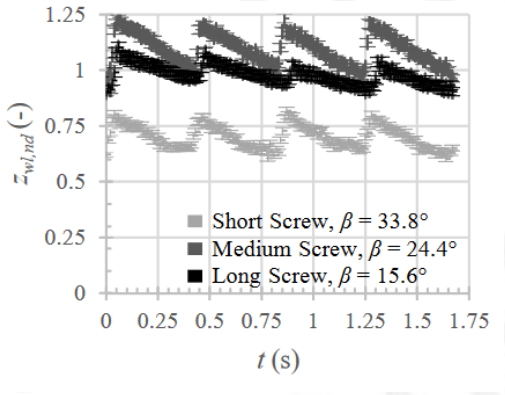

Figure 8: non-dimensional water depth in screw buckets ($z_{wl,nd}$) changing with time (t) for 10 L/s flow at the most efficient operating point for each inclination – measured with pressure tap sensor on the short, medium, and long screw's troughs during operation.

It should be noted that the measurements of the water depth in the shortest screw ($\beta = 33.8°$) did not seem to match up to the bucket fill levels observed visually during the screw's operation. The measured fill heights in this case seemed lower than expected based on visual observation. It is suggested that the pressure tap was installed at a location that did not have fully formed buckets (i.e. either too high or too low along the trough). The short screw has a pitch ratio of $\mathrm{S/L} = 0.80$, which indicates that the screw is not much longer than one full revolution of a flight. When this screw was operating, there was little time between the inrush of water at the formation of the bucket and the exit of water from the bottom of the bucket. Essentially, the screw was too short, and a quasi-steady state bucket of water could not form in the middle of the screw.

This brings up an important point when working with steep inclination screws: as the inclination angle increased and the screw shortened there was much less length along the screw axis for the buckets to fully form and properly extract a torque from the water. Additionally, the slope of each

sawtooth in Figure 8 is proportional to the inclination angle of the screw. This is because the pressure tap measured the fill height from the highest point to the lowest point of the bucket as it passed by, and since the free surface formed along the horizontal plane, the angle of the trough to the free surface was equal to the inclination angle.

This plot demonstrates some phenomena that were observed by the experimenter: the longer screw with less inclination had a more moderate sawtooth pattern and so it was less susceptible to overflowing in its optimal operating range. As well, the experimented noted that the torque in the system oscillated. The measured instantaneous torque varied depending on the position of the buckets in the screw. It was observed that the torque was lower while the initial bucket was forming at the top of the screw. As the bucket formed and translated down the trough, the torque increased to a point when a new top bucket began to form. A similar effect was noticed with the CFD simulations and will be discussed further in Section 5.

4. Computational Fluid Dynamics Model

A three-dimensional, transient, two-phase Reynolds-Averaged Navier Stokes (RANS) CFD model of an Archimedes screw system was developed at the ICUBE Laboratory (Strasbourg, France). Details of governing equations and overall formulation are given by (Dellinger et al. 2018a). Generally, an Euler scheme was used for time discretization, while second order central schemes were used for Laplacian and gradient discretization. The divergence of the velocity was discretized using a second order upwind scheme. Finally, to address the transient nature of the problem, an adaptive time step was implemented, with typical values on the order of 10^{-4} s.

The CFD model was implemented in OpenFOAM 4.1 using the dynamic mesh functionality (cf. Figure 9). The model was built with upper and lower basins connected by a dynamic mesh containing the screw and trough. The dynamic portion of the mesh simulated the rotation of the screw within the fixed

trough and was connected at the top and bottom ends to the upper and lower basin through arbitrary mesh interfaces (AMIs). A small gap was included between the screw's blade tips and the trough to match the experimental setup. This allowed the simulation to account for gap leakage losses.

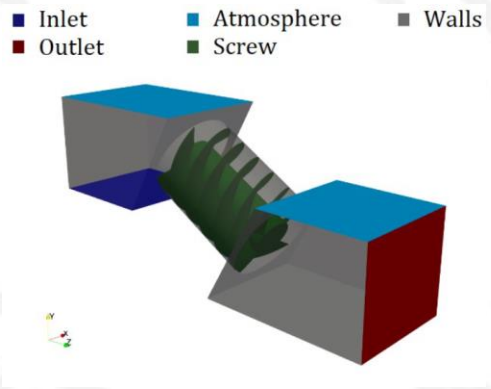

Figure 9: dynamic mesh CFD model of Archimedes screw generators (Dellinger et al. 2018a) with boundaries highlighted. Inlet boundary (dark blue) is shown to upwell flow into the upper basin reservoir where it passes through the screw (green) into the lower basin and into the outlet (red). The atmospheric boundaries are shown in light blue, all other boundaries are stationary walls.

The flow inlet was implemented as uniform upwelling from the base of the upper basin reservoir. An overall flow rate of 10 L/s was used to match the experiments. The arrangement was like the experimental apparatus, in which water flowed into the upper basin, developed a fill height based on the flow rate and rotational speed of the screw, and entered the screw through the top inlet. The fill height of the buckets that formed within the screw was dependent on the water level of the upper basin, the rotational speed of the screw, and the flow rate of the water in the system. After travelling down the screw as buckets, the water exited into the lower basin. The lower basin water level was set to submerge 60% of the screw outlet (i.e. $h_L/D_o \cos\beta = 0.60$) by defining the outlet boundary condition in the simulation. The free surface level was set to a constant height at the point of the vertical axis origin in the lower basin.

Menter's Shear Stress Transport model (or k-ω SST) (Menter 1994) was used for turbulent closure in the simulation and wall functions were used to simulate the effects of the trough and moving blade wall

boundaries. SST turbulent closure was applied to the simulation due to the relative importance of mesh size in the Archimedes screw; a gradient was applied along the blade tips to appropriately model the gap region between the blades and the trough. The SST model is a weighted function that can switch between the k-ω model (at the wall) and the k-ε model (in the log layer) to improve accuracy; this provided a desirable "robustness" to more accurately model the gap region. As well, Menter's Shear Stress Transport model is one of the most commonly used and widely verified models in hydropower turbine modelling (Dhakal and Walters 2010).

The atmospheric boundaries were set to allow the flow of air and water out of the system, and air into the system to keep it operating at atmospheric pressure. The mesh was constructed with refinement along the blade tips so the gap region could be modelled without significant changes in the mesh's aspect ratio. The flow rate and rotational speed of the screw were defined to match the experiments. After all the conditions were defined for a specific test case, the simulation was run until it reached convergence for its torque measurements (Figure 10). OpenFOAM's "forces" post processing utility was used to find the forces and moments of the screw – the moments were transformed and taken as torque about the screw's inclined rotational axis. The overall torque as a function of time was sampled and plotted to see if the simulation had reached convergence. Once a converged value was reached for the torque, the simulation concluded and the last timestep was recorded. Figure 10 shows that the simulations reached convergence at a regularly-oscillating state – termed quasi-steady-state.

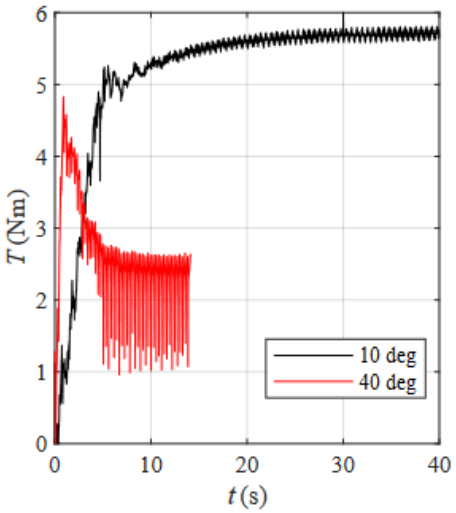

Figure 10: simulation convergence is checked by finding the quasi-steady state period of operation for the screw's torque measurements (T) - here depicted for the shortest and longest simulated screw's (i.e. β = 40° and 10°, respectively). The instantaneous torque is plotted over time(t).

The simulations converged when the same volumetric flow rate of water was entering and exiting the system. The screw was required to fill its bucket volumes and reach a quasi-steady torque to satisfy convergence.

A mesh sensitivity study was carried out to determine the acceptable mesh resolution for the study. Five different levels of refinement were simulated, the results are plotted in Figure 11.

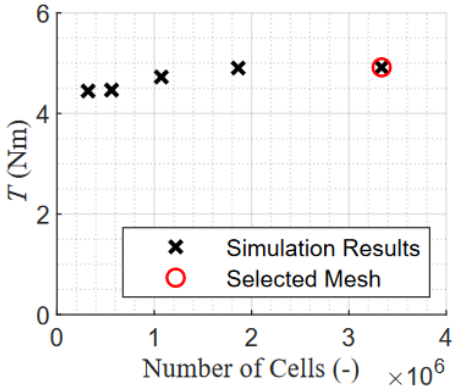

Figure 11: sensitivity study for CFD model. The simulated torques (T) are compared against the level of mesh refinement (i.e., number of cells). The data point corresponding to the selected mesh marked with a red circle.

Figure 11 shows that the mesh resolution converged with 1862828 cells. The mesh with 3335920 cells was selected for the simulation since it did not require much additional computation time but yielded much higher resolution results.

Since the steeper inclination screws were shorter (and had less volume) they reached convergence quicker. The less inclined screw had much less amplitude in its oscillation than the steeper screws. Experimentally, it was observed that torque was not constant during operation since the screw had discreet blades and the buckets formed and emptied; however, the effect was small and relative to experimental uncertainty. However, the torque settling time plot (Figure 10) demonstrated the variance in instantaneous torque for the longest and shortest simulated screws ($\beta = 10°$ and $40°$, respectively) via numerical simulation. The magnitude of the oscillations in torque (and by extension, power production) were higher for the $\beta = 40°$ screw than for the $10°$ screw. This was largely due to the change in volume of the first and last bucket during the filling and emptying phase of the screw's rotation. When the screw was carrying the most volume in its cycle it produced the most torque, but when it was filling up its top bucket and emptying out its bottom bucket, there was a point where it operated at its most empty state and produced the least torque. Shorter screws have fewer buckets that form along the screw during operation, and so the first and last bucket have a proportionally larger effect on overall screw power production than a longer screw with a shallower inclination. This suggested that electrical control circuits might be more complicated for shorter screws since they must deal with large oscillations in power production during operation.

4.1 Validation Study

Three runs from the experimental data were selected for a validation study since the head values were constant throughout the tests. Other comparisons in a previous paper presented by the authors were made with experimental efficiency measurements since the same screw was used for all tests,

meaning that the overall head changed (since the length did not) (Dellinger et al. 2018b). In this case, keeping the head constant allowed for further exploration into the inclination angle's effect on power production, and it allowed for more direct comparisons across the dataset.

Finding points with matching heads between the experimental tests was difficult since the upper water level was not directly set; it depended on flow and screw rotational speed. To account for this, the experiments were carried out with small changes to the rotational speed to gather data across a wide range of changing head values. The results of these high-resolution measurements were then processed to find the rotational speed corresponding to the desired upper water level (h_U). The desired head difference across the screws was $\Delta H = 0.180\ m$; this value occurred for the short screw at 35 RPM, the medium screw at 32 RPM, and the long screw at 38 RPM. These three data points were used to verify the CFD study's accuracy. The lower water level (h_L) was set at a height corresponding to 60% outlet submergence and was kept constant throughout the test – just like the experiments.

Figure 12 shows the comparisons between the simulated values and the experimental values. The simulations agree reasonably well with the experimental results. The convergence is very close for the 15.8° simulation, but the difference between simulation and experimental values is much more evident in the higher inclination screws. These results are consistent with prior validation studies of the CFD model in similar test cases (Dellinger et al. 2018b).

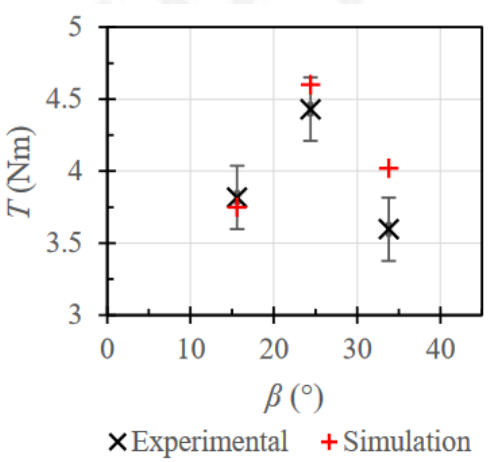

Figure 12: validation data for CFD model. The measured and simulated torques (T) are compared for each inclination angle (β) tested.

The experimental torque measurements have an uncertainty of ± 0.22 Nm. The simulation agrees within the experimental uncertainty for the $\beta = 15.8°$ and $24.4°$ simulations but not for the $\beta = 33.8°$ simulation. This deviance may be explained by a few factors: the simulation does not account for bearing losses, the weight of the screw and net buoyant force, and other mechanical losses in the system.

In the experimental apparatus, a sealed deep-groove ball bearing was used for the lower bearing, and a spherical roller bearing was used for the upper bearing of the screw. Both bearing arrangements were designed to handle some axial loading but have more losses as axial loads increase (Norton 2011). Shallower inclination screws have more proportion of their weight distributed at the bearings as radial loads. Much of this weight was counter-acted by the net buoyancy of the partially submerged screw since it had a sealed, hollow cylindrical tube for its inner diameter. The axial force on the bearings increased as the screw inclination steepened, and bearing losses increased.

4.2 Model Runs

Table 3 shows the dimensions of the screws for the extended screw geometry set as well as the number of control volumes (CVs) used in each simulation. The bolded row matches the $\beta = 24.4°$

394 experimental lab screw, and the other lines at $\beta = 10°, 15°, 20°, 30°, 35°$, and $40°$ are all screw
395 geometries that were created for the CFD simulations. The input values of flow rate, fill height ratio, and
396 head were kept constant at $Q = 10\ L/s$, $f = 1.0$, and $\Delta H = 0.191$ m for the simulations. Mesh
397 sensitivity analysis for the CFD model used in the paper are included in Section 4.5 of Dellinger et al.
398 (Dellinger et al. 2018a). The number of control volumes varied across each simulation since the mesh
399 implemented for each screw was scaled to have the same cell size across all simulations.

400 The length was the only dimension changed amongst the various screw geometries so that a
401 constant geometric head was maintained. The rotational speed was the only operational setting that
402 was changed to maintain a constant fill height ratio of f = 1 across all studies. It was shown in the
403 literature that the most efficient operating point of an ASG will be close to f = 1 (Nuernbergk 2012).
404 Though a bucket fill height of f = 1 might not correspond to exactly the highest efficiency operating point
405 for a screw generator (cf. Figure 5), it does offer a fair comparison across the range of simulated screws
406 as they were each filled with their respective maximum bucket volumes. Overall, the performance of an
407 ASG with full buckets ($f = 1$) provided a strong characterisation of overall screw performance and a way
408 to fairly compare different screw geometries.

409 A performance model for Archimedes screws (Lubitz et al. 2014) was used to make a first guess at
410 the rotational speed and lengths for each simulation of the extended set of Table 3. The simulations
411 were run until convergence and checked to see if they met the head and fill height constraints. Some
412 simulations were run again with a new screw length to meet the head and fill height requirements of
413 the study; the final screw lengths are shown in Table 3. The results of this testing are presented in the
414 following section.

5. Simulation Results

The results from each simulation in Table 3 were post-processed to find the total shaft torque, the inlet water level, and the overall head. The mechanical power available at the screw shaft (termed the "shaft power") is the product of torque and rotational speed (in rad/s). The hydraulic power (or power available in the water) was calculated using the known head and flow rate. The mechanical efficiency of the screw was calculated as

$$\eta = \frac{T\omega}{\rho g Q \Delta H} \tag{2}$$

where the density of water $\rho = 998\ \mathrm{kg/m^3}$, gravitational constant $g = 9.81\ \mathrm{m/s^2}$, T is shaft torque and ω is screw rotational speed in rad/s. The shaft power and mechanical efficiency for each simulated case are shown Figure 13.

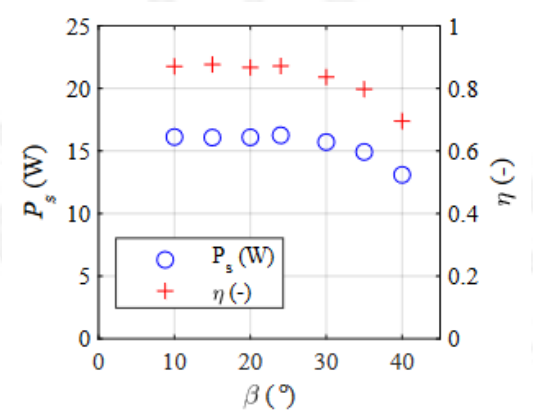

Figure 13: simulation results for shaft power (Ps) and mechanical efficiency (η) with respect to inclination angle (β).

Figure 13 shows that there was a region of almost-constant efficiency between 15° and 24.4°. The power production and efficiency decreased as the slope increased past this range. It was observed that the buckets had less volume of water when full and exhibited more overflow leakage as the inclination steepened (cf. Figure 7). Based on these results it would be reasonable to suggest the optimal inclination

angle for power production is within the range of 15° and 24.4°. It is noted that other practical factors play a role in selecting the optimal inclination angle – these will be discussed in the following section.

It was desired to isolate the power production results from the rotation speed for further investigation. Since mechanical power is a product of the torque and rotation speed (i.e. $P = T\omega$), Figure 14 presents the torque with respect to inclination angle; which is analogous to power production results independent of rotation speed. Isolating for the torque was desirable since the rotation speed varied with the inclination angle to maintain a bucket fill height of $f = 1$ across all simulations for the constant head and constant flow rate.

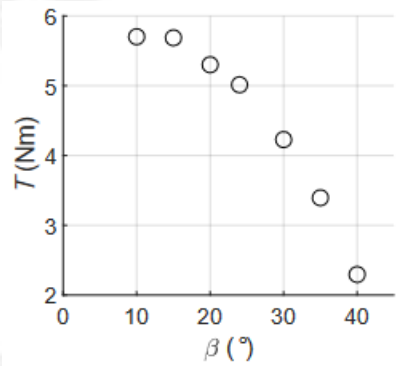

Figure 14: power-generating torque (T) variation with inclination angle (β).

There is an obvious trend in decreasing torque as the inclination angle increased. This demonstrates that screws with a high inclination angle must operate at higher rotational speeds to maintain a similar flow rate and power production. This is because screws with high inclination angles have less capacity in each bucket (cf. Figure 7), therefore they produce less torque. The more deeply inclined, smaller buckets tend to fill faster, and so the screw must operate at higher rotational speeds to reduce overflow leakage losses. There is a balance between speed and power production however: as the speed increases the screw can accommodate more flow rate, but the turbulent and frictional losses increase as well.

The results of the simulations are shown in Table 4 with some additional columns to aid in further discussions. The inclination angle (β), screw length (L), percent change in screw length (ΔL), head difference (ΔH) , flow rate (Q), shaft power produced (P_s), the change in volume of water (where $\alpha = 1$ is the water phase) in the screw based on the inclination angle ($\Delta(\alpha \times V_s)$), and the percent change in the wetted surface area in the screw (ΔA_w) with $\beta = 24.4°$ as the origin for the difference measurements. The rotation speed (Ω) and blade tip speed (ω x R) are also presented to give context to the velocity of the boundaries and better visualize the effects of frictional loss ($P_{L,f}$) as the inclination changed.

Table 4 demonstrates that there were significant increases in length, overall volume, and wetted surface area as the inclination angle decreased. These results helped to suggest a reason for the "constant efficiency" region shown in Figure 13. This phenomenon was very likely due to the changing minor losses in the screw. As the screw's inclination angle decreased (and the screw lengthened) more volume was entrapped in the buckets and there was more surface area for the blades to convert the flow and head into mechanical power. However, a larger surface area also increased frictional losses in the system.

In the simulations, the least friction loss was observed in the $\beta = 20°$ screw. Above this inclination, frictional loss was most effected by the velocity and increased with the inclination. Below this inclination, frictional loss was most effected by surface area and increased as the inclination decreased. It is possible that the increase in power conversion by the longer, less inclined screws was counter-balanced by the increase in frictional losses in this particular region of inclination angles (i.e. $\beta = 10°$ to $24.4°$).

6. Discussion

This section will discuss the theories and practical applications of this paper. Theories will be presented to explain some phenomena exhibited in the experiments and simulations, and the results will be used to suggest a practical optimal inclination angle.

6.1 Initial flow-varying experiment

In the initial flow-rate-varying experiments on the medium screw (presented in Figure 5), it was noted that the highest efficiency point seemed to shift to a higher rotational speed as the flow rate increased. It is suggested that this was because the higher flow rates fill the inlet bucket of the ASG faster. Since the buckets fill faster, they translate down the screw at a faster rate to avoid over-filling at the inlet. If the bucket was under-filled (i.e. the rotational speed was too high to fill the bucket to its maximum volume for the current flow rate) the screw would underperform since it was converting hydrostatic pressure from a smaller volume of water than it was capable of. If it is over-filled (i.e. the rotational speed is too low) water will overflow from each bucket into the successive buckets causing a loss in the system. It is very important that the screw has an optimal filling pattern, which is why it is common to see variable speed ASGs installations in real-world applications (Fergnani and Silva 2016).

6.2 Inclination angle experiments

A similar shift in the highest efficiency point occurred in the inclination experiments. Specifically, Figure 6 showed that screws at higher inclination angles exhibited a shift in maximum efficiency. More steeply inclined screws must operate at higher rotational speeds to maintain high efficiencies. It is suggested that this is mainly due to the changes in geometry of the screw as the inclination angle increased – as Figure 7 showed. When the inclination angle increased the volume of water in the screw decreased; however, the steeper screws filled to their maximum volume faster. So, as ASG rotation speed increased, a shallower inclined screw was not able to fill its bucket volume to a similar level as the

steeper screw – leading to the slight advantage in performance of steeper screws in the high-speed range. In contrast, a less inclined screw has more surface area for viscous friction to act on. Since wall shear stress increases with the square of velocity, this can also explain why the steeper screws may be more efficient at higher rotation speeds.

6.3 Simulations

Based on Figure 4 and the results shown in Table 4, it is suggested that the civil infrastructure of an ASG plant will be significantly altered based on the inclination angle. The most obvious effect is the shortening of the screw as the inclination angle steepens; in this instance there will be less civil infrastructure required to construct a screw plant. Another change due to the inclination angle is the placement of the screw's inlet. It was found that the inlet water level required to provide constant flow varied significantly with inclination angle (Figure 15). And so, the height at which the top of the screw is placed with respect to the weir varies with the inclination angle as well, requiring other adjustments to the civil infrastructure of a screw plant.

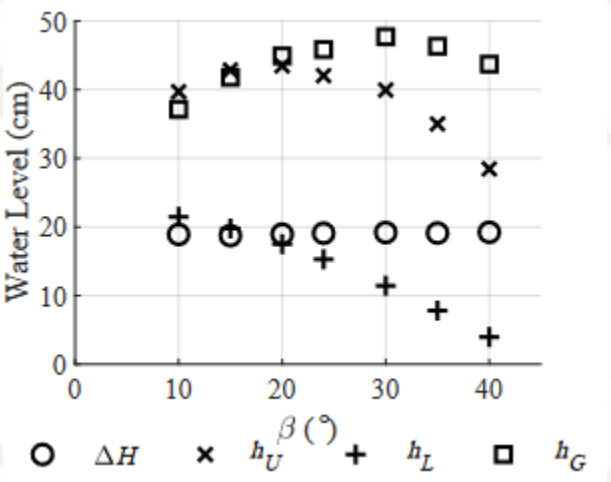

Figure 15: variation of upper water level (hU), lower water level (hL), and geometric head (hG) with inclination angle (β) for a constant head of ΔH = 19.1 ± 0.1 cm and a constant flow rate of Q = 10 L/s.

The inlet water level depends on screw inclination, rotational speed, and flow rate. As screw inclination angle changed, the geometry of the screw inlet changed, which varied the minor head losses at the inlet and changed the upstream water level (i.e. the inlet water level). As well, when the inclination angle increased, the screw rotation speed was also increased which removed some resistance to upstream flow. Thusly, as screw inclination angle increases, the inlet water level should decrease to maintain a constant rate of filling in the buckets. However, it should be noted that the inlet water level first increases for $\beta = 10°$ and $\beta = 15°$ before decreasing across the remainder of the range. It is suggested that this phenomenon was due to the change in losses at the inlet. As the inclination angle changed, the cross section at the inlet changed which varied the entrance losses at the screw's inlet. This might be less prevalent at higher inclination angles since they have respectively higher rotation speeds. At higher speeds, the screw acts as though it has less resistance to flow.

In practice, the inlet water level cannot be modified directly since it is set at the available water level – usually with respect to the height of an adjacent weir. So, to reach a desirable inlet water level, a screw with a steeper inclination should be installed higher than a shallower inclined screw, with respect to weir height. Figure 16 demonstrates that the inlet water level (h_U) is smaller for an ASG with a steep inclination angle, and that the centre pivot offset (C_{po}) must be higher to ensure the level of water at the weir will not flood the screw at its inlet.

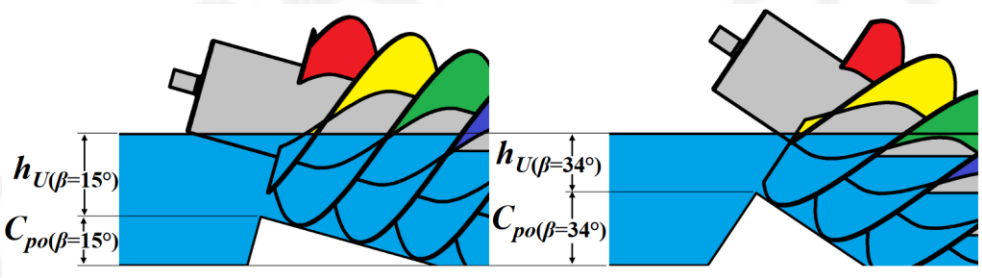

Figure 16: inlet water level and centre pivot offset for a screw with an inclination of β = 15° (left) and β = 34° (right).

Placing the screw at the correct elevation with respect to weir height is essential. If the screw is placed too low (the inlet water level is too high) than it will flood at its inlet. Conversely, if the screw is placed too high (the inlet water level is too low) it will be starved at its inlet. Many real-world installations will adjust the inlet water level by opening or closing a sluice gate at the start of the delivery channel. While this is practical solution if the screw inlet was installed too low, designing the installation with the correct height in the first place will have it performing optimally – utilizing the full available head and discharge of the installation when possible.

6.4 Practical applications

While the long screw ($\beta = 15.6°$) was the most efficient in these experiments – and longer screws were most efficient in the simulations – there are likely other reasons why long screws with correspondingly low inclination angles are not implemented in real-world installations. Firstly, these experiments were carried out on laboratory-scale ASGs. It is expected that the minor losses, friction losses, and bearing losses in the system will scale up to have a different effect in a real-world installation. The $\beta = 15.6°$ screw is 100% longer than the $\beta = 33.8°$ screw for the same head, and while this is only about a 50 cm different in the lab, it is a difference of tens of meters for a full-scale screw with a rated power on the order of 100 kW.

Commonly observed inclination angles of $\beta = 22°$ in full-scale ASGs may make for a more economically efficient installation. There is a lot of expense in lengthening a screw. First and foremost is the civil infrastructure; a less-inclined, longer screw costs more to install. The screw itself requires changes to the manufacturing process (larger work holdings), more materials for the screw and civil infrastructure, a longer frame, and possible changes to bearing arrangement and fixturing. So, though a longer screw may prove to be the most mechanically efficient, shortening the screw to a less-than-optimal power producing inclination angle may prove to be more economically efficient overall.

549 In practise, ASG construction costs would be minimized to maximize the return on investment for a
550 site owner. Since screw and infrastructure costs increase as the inclination angle decreases (and the
551 screw becomes longer) this suggests that ASG installations should be built at inclination angles between
552 approximately $\beta = 20°$ to $25°$. In these simulations, the $\beta = 20°$ simulation efficiency ($\eta = 85.0\%$) was
553 essentially identical to the $\beta = 25°$ case ($\eta = 84.8\%$). Since the $\beta = 20°$ screw was 13.2% longer than
554 the $\beta = 25°$ case, there is potentially a significant cost savings installing the steeper, shorter screw
555 (depending on the scale of the installation) than there is increased power production in implementing
556 the longer screw.

557 This leads into the issue of scaling. This study was carried out on laboratory-scale Archimedes screw
558 generators with outer diameters of $D_o = 0.381\ m$, a head difference of $\Delta H = 0.18$ to $0.19\ m$, and a
559 flow rate of $Q = 0.010\ m^3/s$. Table 1 shows that a small real-world ASG site (Fletcher's Horse World)
560 has an outer diameter of 1.4 m, a head difference of about 1.7 m and a flow rate of about 0.54 m^3/s. A
561 larger installation, like the Valpagliaro Plant, has an outer diameter of 3.6 m, head of 3 m, and flow rate
562 of 5.5 m. Some plants are even larger, like the Widdington plant on Linton Lock (Yorkshire, England),
563 which has an outer diameter of 5 m and was the largest screw plant in the world at time of construction
564 (Landustrie Sneek BV 2017).

565 Generally, the power available for energy conversion is a function the flow rate and the head at the
566 site (i.e. Eq. 2). As the scale of the screw increases (as the diameter and length), the volume of water
567 that the screw can hold increases to the third power. This means that power production will scale to the
568 third power of the length-scale of the plant (i.e. diameter and length).

569 Conversely, losses due to fluid friction are due to the wetted area of the screw, and inflow and
570 outflow losses are due to the cross-sectional area of the screw. Each of these area measurements

increase as a function of the square of the screw's length-scale. So, the laboratory-scale screws are expected to have proportionally larger friction and entrance losses, than a full-scale screw.

Similarly, the gap leakage and overflow leakage losses are expected to change with the scale of the installation. The gap leakage is theorized to scale by the same order as the diameter (Lubitz 2014), or as diameter to the power of 1.5 (Nagel 1968). So, the gap leakage is expected to contribute a very small proportion to the overall system losses as the scale-size of the installation increases. Current models predict the overflow leakage as a function of bucket water level (Nuernbergk and Rorres 2012; Songin and Lubitz 2018). By extension, the overflow leakage scales as the length-scale to the power of 2.5, and so the overflow leakage also scales at a lower rate than the overall power production.

Essentially, the all the major fluidic losses in the system scale to a lesser power than the power production, and so the overall power production of a larger-scale plant is higher than that of a small, laboratory-scale screw. The authors have planned follow-up research into the effects of scaling on Archimedes screw power production and losses.

7. Conclusions

This study gave several important insights into Archimedes screw generator operation and installation. The experiments showed that for a given available head and flow rate, installing an Archimedes screw generator with a lower inclination angle can result in more efficient operation. In the case of the laboratory study, the laboratory-scale screw with an inclination angle of $\beta = 15.6°$ (the "long screw") produced the most power at the highest efficiency. It had these results when compared to similar screws that were identical in every parameter except length and installed at inclination angles of $\beta = 24.4°$ and $33.8°$ (termed the "medium" and "short" screws, respectively). The long screw outperformed the short screw outside the realm of experimental uncertainty, but performance of the medium and long screw was not notably different with the range of experimental uncertainty. This

suggested that both the long and medium screw performed similarly. These data points were then used to validate a CFD model, which was implemented to extend the dataset.

The CFD results agreed well with the experimental measurements, diverging slightly at high inclination angles. It was suggested that this divergence was due to the exclusion of bearing loss and buoyancy in the CFD models, since these phenomena will likely have a greater impact at high inclination angles. Overall, the divergence was still relatively low, and the model was sufficiently accurate to use to examine the effect of by the authors, particularly since the divergence was occurring within the high range of inclination angles that had been shown to be impractical and have poor performance experimentally.

The CFD model was then used to extend the dataset for laboratory-scale ASG installations with constant head, constant flow rate, and a bucket fill height ratio of $f = 1$. It was found that the mechanical power produced at the shaft (i.e. the power available for conversion by the generator) reached a plateau for inclination angles between $\beta \approx 15°$ and $25°$ - which was like the results of the experiment. The authors note that the most mechanically efficient screw may not necessarily be the most economically efficient screw. Since the data returned results so similar in power production for this range of inclination angles, it is suggested that the steepest of these inclination angles is optimal (i.e. $\beta \approx 25°$). A steeper inclination angle will minimize the cost of materials and civil infrastructure.

It should be noted that these results were found for laboratory-scale screws and might differ as the size of the ASG installation increases. Future research plans include investigating the effect of scaling of hydropower systems between laboratory and full-scale sizes. This paper discussed Archimedes screw generators at the laboratory scale, but real-world installations are much larger and experience different scales of fluid mechanics.

8. Data Availability Statement

Some or all data, models, or code generated or used during the study are available from the corresponding author by request.

9. Acknowledgements

Aspects of this work were financially supported by the Natural Sciences and Engineering Research Council (NSERC) Collaborative Research and Development (CRD) program (grant # CRDPJ 433740-12) and Greenbug Energy Inc. (Delhi, ON, Canada). The assistance of Tony Bouk and Brian Weber of Greenbug Energy Inc. is gratefully acknowledged.

10. Notation

A_w = wetted area of screw (m^2);
C_{po} = centre-pivot offset (m);
D_i = inner diameter (m);
D_o = outer diameter (m);
f = fill height ratio (-);
g = gravitational constant (9.81 m/s^2);
G_w = gap width (m);
ΔH = overall head (m);
h_G = geometric head (m);
h_L = lower water level (m);
h_U = upper water level (m);
L = flighted length (m);
N = number of blades (-);
P_s = mechanical power at the screw's shaft (W);
$P_{L,f}$ = power loss due to friction (W);
Q = flow rate (m^3/s);
R = outer radius (m)
S = screw pitch (m);
T = torque (Nm);
V_b = bucket volume (m^3);
V_s = volume within screw's flights (m^3);
z_{min} = minimum bucket water level (m);

z_{max} = maximum bucket water level (m);
z_{wl} = bucket water level (m);
$z_{wl,nd}$ = dimensionless bucket water level (-);
α = fluid phase, $\alpha = 1$ (water), $\alpha = 0$ (air);
β = inclination angle (°);
η = efficiency (-);
ρ = water density (998 kg/m^3);
ω = screw rotation speed (rad/s); and
Ω = screw rotation speed (RPM);

11. References

Dellinger, G., Garambois, P.-A., Dellinger, N., Dufresne, M., Terfous, A., Vazqueza, J., and Ghenaimb, A. (2018a). "Computational fluid dynamics modeling for the design of Archimedes Screw Generator." Renewable Energy, 118, 847–857.

Dellinger, G., Garambois, P., Dufresne, M., Terfous, A., Vazquez, J., and Ghenaim, A. (2016a). "Numerical and experimental study of an Archimedean Screw Generator." 28th AHR Symposium on Hydraulic Machinery and Systems, Grenoble, July 4-8, 2, 1419–1428.

Dellinger, G., Simmons, S., Lubitz, W. D., Garambois, P.-A., and Dellinger, N. (2018b). "Effect of slope and number of blades on Archimedes screw generator power output." Renewable Energy, (Online January 2019).

Dellinger, G., Terfous, A., Garambois, P.-A., and Ghenaim, A. (2016b). "Experimental investigation and performance analysis of Archimedes screw generator." Journal of Hydraulic Research, 1686 (April).

Dhakal, T. P., and Walters, D. K. (2010). "Curvature and Rotation Sensitive Variants of the K-Omega SST Turbulence Model." ASME 2009 Fluids Engineering Division Summer Meeting, ASME, Vail, Colorado, 2221–2229.

Fergnani, N., and Silva, P. (2016). "Technical and economic assessment of an Archimedean screw with variable speed operation under variable flows." Energy Department of Politecnico di Milano, Milan. Report.

645 Havn, T. B., Sæther, S. A., Thorstad, E. B., Teichert, M. A. K., Heermann, L., Diserud, O. H., Borcherding, J.,
646 Tambets, M., and Økland, F. (2017). "Downstream migration of Atlantic salmon smolts past a
647 low head hydropower station equippped with Archimedes screw and Francis turbines."
648 Ecological Engineering, Elsevier B.V., 105, 262–275.

649 Hawle, W., Lashofer, A., and Pelikan, B. (2012). "Lab Testing of the Archimedean Screw." Proc.
650 Hidroenergia 2012, Hidroenergia, Wroclaw, Poland.

651 Khan, A., Simmons, S., Lyons, M., and Lubitz, W. (2018). "Inlet Channel Effects on Archimedes Screw
652 Generators." Proceedings of The Canadian Society for Mechanical Engineering International
653 Congress 2018, CSME, Toronto, Canada.

654 Kibel, P. (2008). "Archimedes Screw Turbine Fisheries Assessment. Phase II: Eels and Kelts." Fishtek
655 Consulting Ltd. (UK), Moretonhampstead, Devon. Report.

656 Kozyn, A. (2016). "Power Loss Model for Archimedes Screw Turbines." University of Guelph. MASc.
657 Thesis.

658 Kozyn, A., Ash, S., and Lubitz, W. D. (2015). "Assessment of Archimedes Screw Power Generation
659 Potential in Ontario CCTC 2015 Paper Number 1570095585." (1570095585), 1–11.

660 Landustrie. (2017). "Hydropower: Linton Lock (UK)." Landustrie.nl,
661 <https://www.landustrie.nl/en/products/hydropower/projects/linton-lock.html> (Mar. 3, 2020).

662 Lashofer, A. (2019). "Projekt Wasserkraftschnecken Verortung." Ingenieurbüro Lashofer,
663 <https://www.lashofer.at/deutsch/wasserkraftschnecke/projekt-wasserkraftschnecken-
664 verortung/>. Web Page.

665 Lashofer, A., Hawle, W., and Pelikan, B. (2012). "State of technology and design guidelines for the
666 Archimedes screw turbine." University of Natural Resources and Life Sciences Vienna (BOKU),
667 (October), 1–8.

668 Lisicki, M., Lubitz, W., and Taylor, G. W. (2016). "Optimal design and operation of Archimedes screw
669 turbines using Bayesian optimization." Applied Energy, Elsevier Ltd, 183, 1404–1417.

670 Lubitz, W. D. (2014). "Gap Flow in Archimedes Screws." CSME International Congress 2014, (June), 1–6.

671 Lubitz, W. D., Lyons, M., and Simmons, S. (2014). “Performance Model of Archimedes Screw Hydro
672 Turbines with Variable Fill Level.” Journal of Hydraulic Engineering, 140(10), 1–11.

673 Lyons, M. (2014). “Lab Testing and Modeling of Archimedes Screw Turbines.” University of Guelph.
674 MASc. Thesis.

675 Lyons, M., and Lubitz, W. D. (2013). “Archimedes screws for microhydro power generation.” Proceedings
676 of the ASME 2013 7th International Conference on Energy Sustainability & 11th Fuel Cell
677 Science, Engineering and Technology Conference, Minneapolis, USA, 1–7.

678 McNabb, C. D., Liston, C. R., and Borthwick, S. M. (2003). “Passage of Juvenile Chinook Salmon and other
679 Fish Species through Archimedes Lifts and a Hidrostal Pump at Red Bluff, California.”
680 Transactions of the American Fisheries Society, 132(1985), 326–334.

681 Menter, F. R. (1994). “Two-equation eddy-viscosity turbulence models for engineering applications.”
682 AIAA Journal, 32(8), 1598–1605.

683 Müller, G., and Senior, J. (2009). “Simplified theory of Archimedean screws.” Journal of Hydraulic
684 Research, 47(5), 666–669.

685 Nagel, G. (1968). Archimedian Screw Pump Handbook: Fundamental Aspects of the Design and
686 Operation of Water Pumping Installations Using Archimedian Screw Pumps. RITZ-Pumpenfabrik
687 OHG, Schwäbisch Gmünd.

688 Norton, R. L. (2011). “Bearings and Lubrication.” Machine Design: An Integrated Approach, Prentice Hall,
689 New Jersey, 623–680.

690 Nuernbergk, D. (2012). Wasserkraftschnecken - Berechnung und optimaler Entwurf von archimedischen
691 Schnecken als Wasserkraftmaschine (Hydropower screws - Calculation and Design of
692 Archimedes Screws used in Hydropower). Verlag Moritz Schäfer, Detmold.

693 Nuernbergk, D. M., and Rorres, C. (2012). “An Analytical Model for the Water Inflow of an Archimedes
694 Screw Used in Hydropower Generation.” Journal of Hydraulic Engineering, 139(2),
695 120723125453009.

696 Radlik, K.-A. (1997). “Hydrodynamic screw for energy conversion.” German Patent DE4139134A1.
697 December 4, 1997.

698 Rohmer, J., Knittel, D., Sturtzer, G., Flieller, D., and Renaud, J. (2016). “Modeling and experimental
699 results of an Archimedes screw turbine.” Renewable Energy, Elsevier Ltd, 94, 136–146.

700 Rorres, C. (2000). “The Turn of the Screw: Optimal Design of and Archimedes Screw.” Journal of
701 Hydraulic Engineering, 126(1), 72–80.

702 Simmons, S. (2018). “A Computational Fluid Dynamic Analysis of Archimedes Screw Generators.”
703 University of Guelph. MASc. Thesis.

704 Simmons, S., and Lubitz, W. (2017). “Archimedes screw generators for sustainable energy
705 development.” Proc. IHTC 2017 - IEEE Canada International Humanitarian Technology
706 Conference 2017, Toronto, Canada.

707 Simmons, S., Songin, K., and Lubitz, W. (2017). “Experimental investigation of the factors affecting
708 Archimedes screw generator power output.” HYDRO 2017 (7-11 October 2017), Hydropower
709 and Dams, Seville, Spain.

710 Songin, K. (2017). “Experimental Analysis of Archimedes Screw Turbines.” University of Guelph. MASc.
711 Thesis.

712 Songin, K. J., and Lubitz, W. D. (2018). “Measurement of fill level and effects of overflow in power-
713 generating Archimedes screws.” Journal of Hydraulic Research, 57(5), 635–646.

714

715 **Table 1: dimensions of four full-scale ASG sites by increasing inclination angle and design head. Details of the WKS Marsberg-**
716 **Padberg site are cited from Lashofer (Lashofer 2019).**

Site Name	Location	β (°)	D_o (m)	L (m)	Design Head (m)	Discharge Capacity (m^3/s)	Rated Power (kW)
Fletcher's Horse World	Waterford, Ontario, Canada	22	1.4	4.5	1.7	0.54	7.2
Valpagliaro Plant	Ferrara, Emilia-Romagna, Italy	22	3.6	7.4	3	2 x 5.5	2 x 121
Buckfast Abbey	Buckfastleigh, Devon, England	26	2.5	10.562	4.2	2.8	84
WKS Marsberg-Padberg	Marsberg, North Rhine-Westphalia, Germany	30	2	8.9	4.47	1	37

717

718 **Table 2: laboratory screw dimensions.**

	Symbol	Short Screw	Medium Screw	Long Screw
Number of Blades (-)	N	4	4	4
Inner Diameter (mm)	D_i	168	168	168
Outer Diameter (mm)	D_o	381	381	381
Pitch (mm)	S	381	381	381
Flighted Length (mm)	L	478	617	952
Inclination Angle (mm)	β	33.8	24.4	15.6

719

720

721 **Table 3: geometry and input values for CFD simulations of each inclination angle.**

β (°)	D_o (cm)	D_i (cm)	S (cm)	L (cm)	Number of Blades	Number of Cells ($x10^6$)
10	38.1	16.8	38.1	108.6	4	16.3
15	38.1	16.8	38.1	83.6	4	12.7
20	38.1	16.8	38.1	69.9	4	11.4
24.4	**38.1**	**16.8**	**38.1**	**61.7**	**4**	**9.9**
30	38.1	16.8	38.1	55.1	4	9.7
35	38.1	16.8	38.1	49.3	4	8.9
40	38.1	16.8	38.1	44.4	4	8.8

722

Table 4: Simulation results for each inclination angle. The percent change of the length of the screw (ΔL), change in volume of water in the screw ($\Delta V_{s,\alpha=1}$, where α = 1 is the water phase and V_s is the screw volume), and percent change in wetted surface area of the screw (ΔA_w) are shown for reference.

β (°)	L (cm)	ΔL (%)	ΔH (m)	Q (L/s)	$\Delta(\alpha \times V_s)$ (L)	ΔA_w (%)	Ω (RPM)	$\omega \times R$ (m/s)	P_s (W)	$P_{L,f}$ (W)
10	108.6	76.0%	0.19	10.0	61.0	119.6%	25.3	0.504	16.1	0.281
15	83.6	35.5%	0.19	10.0	35.2	56.3%	27.0	0.539	16.1	0.211
20	69.9	13.2%	0.19	10.0	15.3	21.7%	29.0	0.579	16.1	0.200
24.4	**61.7**	**-**	**0.19**	**10.0**	**-**	**-**	**31.0**	**0.618**	**16.3**	**0.213**
30	55.1	-10.8%	0.19	10.0	-17.0	-22.2%	35.5	0.708	15.7	0.242
35	49.3	-20.2%	0.19	10.0	-30.8	-40.5%	42.0	0.838	14.9	0.322
40	44.4	-28.1%	0.19	10.0	-43.5	-56.3%	54.5	1.087	13.1	0.519

12. Figure Captions

Figure 1: Archimedes screw generator geometry.

Figure 2: the University of Guelph's Archimedes screw laboratory setup. The screw is placed between an upper and lower basin (a) and a VFD motor is mounted on the top end (b) to control speed and measure torque using a strain gauge and torque arm.

Figure 3: maximum (z_{max}), minimum (z_{min}), and actual (z_{wl}) water levels in an Archimedes screw bucket.

Figure 4: from left to right: the long, medium, and short screws shown with their respective lengths and inclination angles.

Figure 5: determining the optimal flow rate and rotational speed (Ω) for the medium length screw and the subsequent studies on both the long and short screws. The mechanical efficiency (η) is plotted against the rotational speed of the installation.

Figure 6: mechanical efficiency (η) with respect to rotational speed (Ω) of the long, medium, and short screws for a 10 L/s flow rate with fill height ratios of $f = 1$ highlighted for reference. The left plot (a) shows the full range of rotation speeds, while the right plot (b) magnifies the plot to show the higher resolution data points clearly.

Figure 7: effect of inclination angle on total bucket volume of a full bucket (i.e. $f = 1$).

Figure 8: non-dimensional water depth in screw buckets ($z_{wl,nd}$) changing with time (t) for 10 L/s flow at the most efficient operating point for each inclination – measured with pressure tap sensor on the short, medium, and long screw's troughs during operation.

Figure 9: dynamic mesh CFD model of Archimedes screw generators (Dellinger et al. 2018a) with boundaries highlighted. Inlet boundary (dark blue) is shown to upwell flow into the upper basin

reservoir where it passes through the screw (green) into the lower basin and into the outlet (red). The atmospheric boundaries are shown in light blue, all other boundaries are stationary walls.

Figure 10: simulation convergence is checked by finding the quasi-steady state period of operation for the screw's torque measurements (T) - here depicted for the shortest and longest simulated screw's (i.e. $\beta = 40°$ and $10°$, respectively). The instantaneous torque is plotted over time(t).

Figure 11: sensitivity study for CFD model. The simulated torques (T) are compared against the level of mesh refinement (i.e. number of cells). The data point corresponding to the selected mesh marked with a red circle.

Figure 12: validation data for CFD model. The measured and simulated torques (T) are compared for each inclination angle (β) tested.

Figure 13: simulation results for shaft power (P_s) and mechanical efficiency (η) with respect to inclination angle (β).

Figure 14: power-generating torque (T) variation with inclination angle (β).

Figure 15: variation of upper water level (h_U), lower water level (h_L), and geometric head (h_G) with inclination angle (β) for a constant head of $\Delta H = 19.1 \pm 0.1$ cm and a constant flow rate of $Q = 10$ L/s.

Figure 16: inlet water level and centre pivot offset for a screw with an inclination of $\beta = 15°$ (left) and $\beta = 34°$ (right).